17th World Conference on Earthquake Engineering, 17WCEE
Sendai, Japan - September 13th to 18th 2020

SENSITIVITY ANALYSIS OF STEEL MOMENT CONNECTIONS WITH SHAPE MEMORY ALLOY BOLTS

M. Mohammadi Nia [(1)], S. Moradi [(2)]

[(1)] *PhD candidate, Department of Civil Engineering, Ryerson University, 350 Victoria Street, Toronto, Ontario, M5B 2K3, Canada, majid.mohammadinia@ryerson.ca*
[(2)] *Assistant Professor, Department of Civil Engineering, Ryerson University, 350 Victoria Street, Toronto, Ontario, M5B 2K3, Canada, s.moradi@ryerson.ca*

Abstract

Shape memory alloys (SMAs) are a class of metallic alloys that exhibit several unique characteristics, such as self-centering, which is the ability of the material to return to their original un-deformed position after experiencing large inelastic deformations. Several past studies have reported on the potential of using SMAs for providing self-centering in structures and thus minimizing permanent deformations, losses, and downtime. One recent application of SMA in steel structures employs superelastic SMA bolts in extended end-plate moment-resisting connections. Both experimental and numerical studies confirm the viability of using SMAs for the self-centering capability of steel connections. To examine the cyclic response of end-plate steel connections with superelastic SMA bolts, a statistical sensitivity assessment of these new connections is performed. The study is based on detailed finite element simulations and the design of experiment method. The finite element modeling, which includes material and geometry nonlinearities as well as pre-tensioned and contact elements, is first validated against past experimental studies. Twenty-one design factors are considered as input parameters for the sensitivity analysis. Sixty-four connection models are analyzed while all the connections meet the seismic design requirements of AISC 341-16 and AISC 358-16 for extended end-plate connections and highly ductile members. The cyclic behavior of SMA-based steel connections is statistically evaluated in terms of different response characteristics, including initial stiffness, moment capacity, hysteretic energy dissipation, and SMA-bolt rupture index. The results determine the relative significance of different design factors on the cyclic behavior of end-plate connections equipped with SMA bolts. Based on the results, the end-plate thickness and bolt diameter are the most significant factors. Using thicker endplates is recommended to reach stiffer connections with high levels of moment capacity and hysteretic energy dissipation. Moreover, the potential for bolt fracture, which is a critical failure mode in SMA-based steel connections, can be reduced by increasing the bolt diameter and by adding stiffeners in the connection. Higher energy dissipation capacity is observed for connections with a larger bolt diameter, deeper beams, thicker endplates, and added stiffener plates. Finally, using bolts with higher diameters is recommended to have stiffer connections; increase the energy dissipation and moment capacities; and reduce the potential for bolt fracture.

Keywords: shape memory alloys; smart materials, self-centering structures, steel connections; finite element analysis

1. Introduction

Steel structures are prone to residual deformations after a severe seismic event. Repairing a damaged structure is difficult, expensive, and sometimes impossible. To avoid repair costs and downtime, researchers propose the idea of self-centering structures where the structure returns to its undeformed shape upon unloading. A self-centering structure can be achieved, for example, by adding pre-tensioned cables or smart materials to the structure. An early study of self-centering connections in steel structures is traced back to post-tensioned connections by Ricles et al [1]. Other than post-tensioned steel frames, controlled rocking steel braced frames [2], and steel frames equipped with shape memory alloy (SMA) bolts [3] are other self-centering systems. Shape memory alloys are a special type of smart materials that are capable to return to their original shape by either heating or unloading.

SMA-based self-centering systems have superiority over other types of self-centering systems, such as controlled rocking steel braced systems and post-tensioned frames. These advantages include having fewer construction efforts and reducing the applied axial force to the beam or column, which may trigger early local buckling [4]. Using extended-end-plate connections equipped with SMA bolts have less installation complexity and floor-slab interference compared to other types of SMA-based connections [5].

Using SMA materials as a tool to achieve a resilient structure has been investigated in the past two decades. Two specimens were tested by Ocel et al. [6]. In the tested specimens, shape memory effect (SME) was used where heating above the transformation temperature is required to reduce residual deformations. High levels of energy dissipation and ductility were observed without any strength degradation. However, the tested specimens were not able to recover the whole residual deformations. Speicher et al. [5] tested four connection specimens. In those specimens, superelastic NiTi shape memory, martensitic nickel–titanium, steel, and superelastic NiTi paralleled with aluminum tendons were used. The results showed that the specimens with superelastic nickel–titanium tendons outperformed in terms of recentering. DesRoches et al. [7] performed a system-level assessment of SMA-based steel frames. Their results indicated that residual deformations and maximum deformation demands can be controlled by superelastic SMA connections and martensitic SMA connections, respectively.

To better understand the behavior of steel moment connections with SMA bolts, a comprehensive study is required with the goal of assessing the effect of different design parameters on the connections' behavior. In this study, a design-of-experiments framework is used to assess the effect of different design parameters on the cyclic responses of SMA-based extended endplate steel connections. To conduct a sensitivity analysis, firstly, a 3D finite element model is developed in ANSYS [8]. The modeling is validated with the results of an experimental study by Fang et al. [3]. Design-Expert software [9] is then used to generate factor combinations. For each design (factor combination), a finite element model is created and analyzed. For each analyzed model four cyclic response variables, including initial stiffness, hysteretic energy dissipation, maximum applied moment, and SMA-bolt rupture index are extracted. Analysis of variance (ANOVA) is performed to evaluate the significance of design factors. In this study, due to the large number of parameters, i.e. 21 factors, a sequential fractional factorial technique is applied where the first round of design combinations are analyzed and based on their results, unimportant factors are identified and excluded in the second round of analyses. Finally, factors of paramount importance and their probable interactions are highlighted to have a better view of the seismic behavior of the SMA-based steel connections. The results from this research are useful for understanding the cyclic behavior of SMA-based extended endpalte connections.

2. Shape Memory Alloy (SMA)

Shape memory alloys (SMA) are metallic alloys with the capability of returning to their original shape upon unloading and/or heating. Superelastic SMAs are capable of undergoing large deformations and returning to their undeformed shape upon unloading. The distinct recentering behavior of SMAs stem from their material microstructure where two unique crystallographic structures exist, namely austenite and martensite. The austenite phase is crystallographically more ordered. The transformation between SMAs' two crystallographic phases provides SMAs with the shape recovery capability.

Among different types of SMAs, *NiTi* or Nitonol is the most common SMA. Manufacturing and training of *NiTi* SMAs are costly, however, they exhibit strong superelasticity and shape memory effect [10]. To reduce the cost of SMAs and make them affordable for industrial applications, different types of SMAs have been proposed. For example, Cu-based alloys are relatively cheap, but their ductility is not as good as Nitonols. As another alternative for *NiTi* SMAs, Fe-Mn-Si-based alloys have been proposed. These alloys have showed good mechanical properties with an acceptable weldability feature and transformation hysteresis [11]. Using iron-based SMAs could be a good option for civil engineering related applications. Nevertheless, further developments are required for large-scale production of the iron-based SMAs [12].

3. Finite element modeling of beam-column connection specimens

ANSYS software [30] is used to develop a 3-D model. The developed model is verified in comparison with two experimental tests reported in Ref. [3]. 3D solid elements (SOLID185) are utilized to mesh the beam, column, endplate, bolts, and washers. Finer meshes are used for the components close to the connection interface, such as panel zone, bolts and part of the beam, where high stress concentrations are expected. Using this meshing increases the efficiency of the computational model. Two specimens are considered to verify the developed model, namely SMA-D16-290, and SMA-D10-240d. Also, a pretension load equal to 65% of the forward transformation stress is applied to the bolts. Fig. 1 depicts the developed model for specimen SMA-D10-240d.

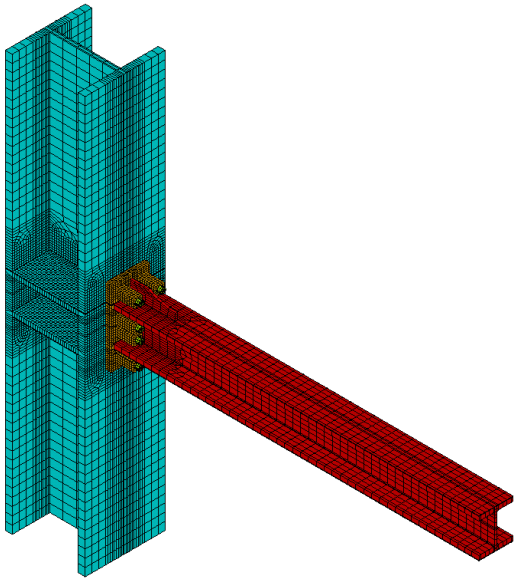

Fig. 1. The developed finite element model for specimen SMA-D10-240d [3]

Table 1 summarizes the material properties in the validation study, which are according to the experimental study by Fang et al [3]. Steel materials are modeled using trilinear stress-strain behavior. The proposed SMA behavior in ANSYS [8] is used to simulate SMA bolts. It is worthy to note that no response degradation is considered in ANSYS [8].

Table 1. Material properties in the finite element modeling [3]

Component	Modulus of elasticity (GPa)	Yield strength (MPa)	Ultimate strength (MPa)
Beam	210.1	287.5	452.9
Column	193.3	306.1	487.4
Endplate	205.6	377.5	531.2

CONTA174 and TRAGE170 are used to define the probable contacts between bolt shanks and holes within endplate and column flange, and the contact between endplate and column flange. Moreover, the developed models capture large deformations, material and geometry nonlinearities. In the contact definitions, the following assumptions are considered;

- Contacts are detected on Gauss points.
- The penalty function is used as the contact algorithm.
- Updated contact stiffness is used, where the stiffness of the contact is updated in each iteration based on current mean stress of underlying elements.
- A friction coefficient of 0.33 is considered for all the contact surfaces.

The cyclic loading is applied at a certain distance, i.e. 1.5 m, from the column face. Welds are not explicitly modeled; however, their effects are considered by constraining the relevant degrees of freedom in the finite element models.

Fig. 2 shows the moment-plastic rotation curves for specimens D10-190 and D10-240d. As shown, the results have a good agreement with experimental results. The plastic rotation is calculated using the following equation:

$$\theta_p = (\Delta - P/K_e)/L \tag{1}$$

in which Δ stands for the displacement at the loading point, P shows the applied load, K_e is the elastic stiffness of the beam, and L indicates the length of the beam. More details about the finite element modeling and simulations are available in [13].

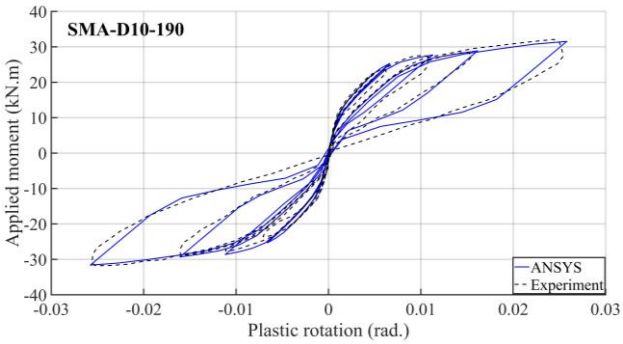

(a)

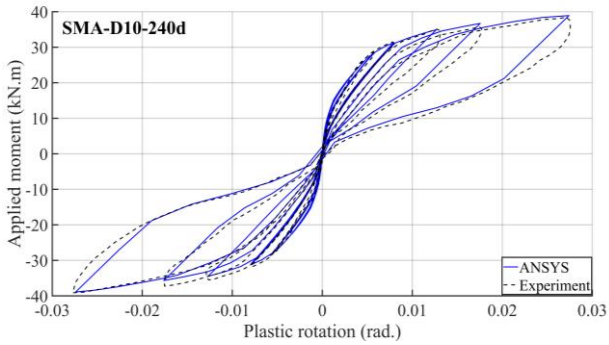

(b)

Fig. 2– Comparison of finite element modeling and experimental results in terms of moment-plastic rotation; (a) specimen SMA-D10-190; (b) specimen SMA-D10-240d

3. Sensitivity analysis

A Design-of-experiment method is used to statistically evaluate the effect of different factors on the cyclic behavior of SMA-based endplate connections. In particular, a two-level fractional factorial design is generated with twenty-one factors as input factors. These factors are selected based on previous research studies. The associated range for each factor is selected to have broad and practical ranges while meeting the requirements of AISC 341-16 and AISC 358-16. In a two-level factorial design, high and low levels are required for each factor. In Table 2, the factors and the associated ranges are listed.

As the number of factors increases, using the sequence of smaller experiments is more efficient where the results from a smaller experiment are extracted, and then they are applied for assessing next computer experiments. Consequently, in this study, two sets of experiments are performed as the initial and secondary analyses. Each round consists of thirty-two factor combinations, which means that the design matrix in this study contains sixty-four models.

Table 2. Factors and associated ranges.

Factor	Symbol	Low level (-)	High level (+)	Unit
Martensite start stress	σ_{Ms}	280	380	MPa
Martensite finish stress	σ_{Mf}	410	590	MPa
Austenite start stress	σ_{As}	170	250	MPa
Austenite finish stress	σ_{Af}	70	138	MPa
Young's modulus of elasticity	E_{SMA}	27	50	GPa
Maximum transformation strain	ε_L	0.05	0.135	-
Bolt pretension stress ratio	F_{pt}	0.5	0.65	-
Bolt length	L_{bolt}	190	290	mm
Bolt diameter	D_{bolt}	10	20	mm
Horizontal distance between bolts	g	140	180	mm
Vertical distance from the outside of a beam tension flange to the nearest outside bolt row	p_{fo}	105	140	mm
Vertical distance from the inside of a beam tension flange to the nearest inside bolt row	p_{fi}	105	140	mm

Endplate thickness	t_p	13	38	mm
Endplate width	b_p	290	350	mm
Endplate yield stress	F_{yp}	355	405	MPa
Stiffener thickness*	t_s	0	25	mm
Beam flange slenderness ratio($b_{bf}/2t_{bf}$)	λ_{fb}	4	6	-
Beam web slenderness ratio (h_{bw}/t_{bw})	λ_{wb}	27.5	38.1	-
Beam length	L_b	3	4.5	m
Column flange slenderness ratio ($b_{cf}/2t_{cf}$)	λ_{fc}	5.3	6	-
Column web slenderness ratio (h_{cw}/t_{cw})	λ_{wc}	16	23.3	-

* The plate located at the top and bottom of the beam, and welded to the endplate and beam flange (Fig.1)

Four cyclic response variables have been considered, including initial stiffness (K_i), maximum applied moment (M_{max}), hysteretic energy dissipation (*HED*), and SMA-bolts rupture index (RI_{bolt}). The initial stiffness response K_i is calculated at 0.375% story drift ratio. Fig. 3 shows a schematic hysteretic response and the recorded response variables. It should be noted that *HED* is recorded for the whole cyclic loading. Also, PI_{bolt} is obtained based on the following equation:

$$RI_{bolt}=EPEQ/exp\,(-1.5\sigma_M/\,\sigma\,) \tag{2}$$

where, σ_M and σ stand for hydrostatic and von Mises stresses, respectively. RI_{bolts} is recorded at 4% story drift ratio for all the nodes within the bolts.

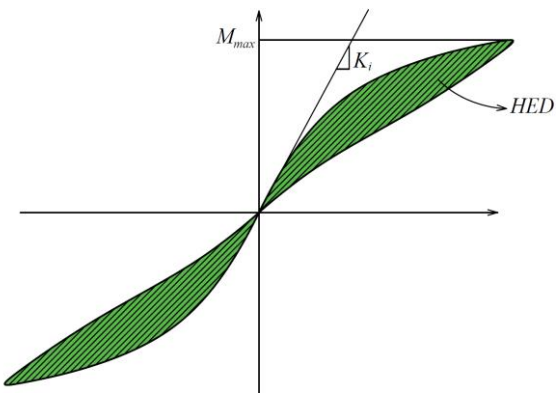

Fig. 3– Schematic view of the recorded response variables

Adding SMA-bolts to the extended endplate connections results in structural recentering capability. This recentering capability is noticed from flag-shape hysteretic moment-rotation curves. Examples of the flag-shape hysteretic responses for models 52 and 58 are shown in Fig. 4.

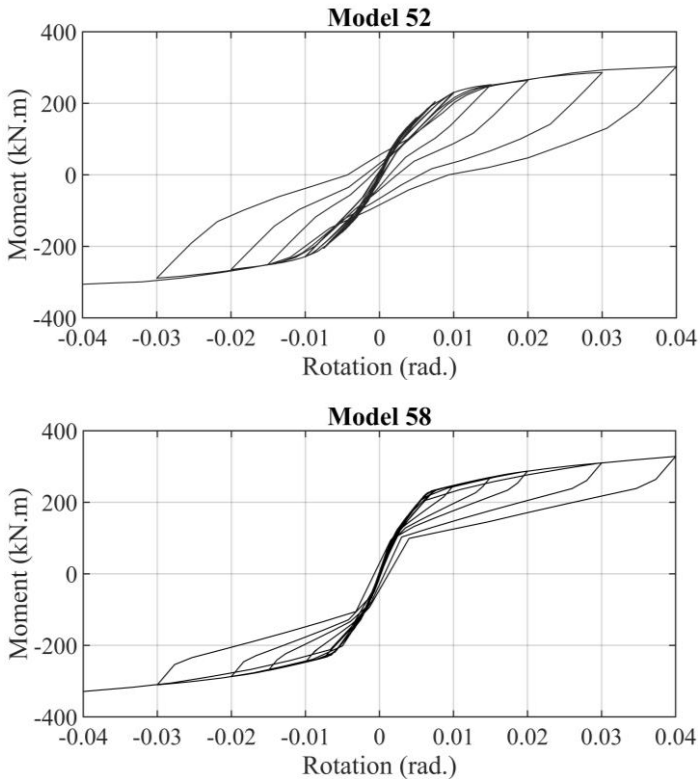

Fig. 4– Moment-rotation responses of models 52 and 58

4. Results and discussions

Significant factors based on sixty-four analyzed models are listed in Table 3. For each response variable, a detailed discussion is provided in the following section. Important factors on the response variables are tabulated in Table 3. For each response variable and its influential factors, the percentage contribution, which is defined as the sum of squares for each factor to total sum of squares [14], are calculated. The percentage contribution is an effective tool for distinguishing the relative significance of the factors. Fig. 5 presents the percentage contributions of different factor and interaction effects. In this figure, factors with a positive effect are shown with a black color, whereas factors with a negative effect are shown with a red color.

Table 3. Significant factors and interactions

Response	Significant factors
Initial stiffness	D_{bolt}; t_p; λ_{bw}; (D_{bolt} t_p); (D_{bolt} λ_{bw}); t_s
Maximum moment	D_{bolt}; t_p; ε_L; λ_{bw}; (ε_L t_p); L_{bolt}
Hysteretic energy dissipation	D_{bolt}; λ_{bw}; t_p; D_{bolt} λ_{bw}; t_s; D_{bolt} t_p
SMA-bolt rupture index	t_p; D_{bolt}; (t_p D_{bolt}); (σ_{Ms} E_{SMA}); (σ_{Ms} ε_L); t_s; ε_L

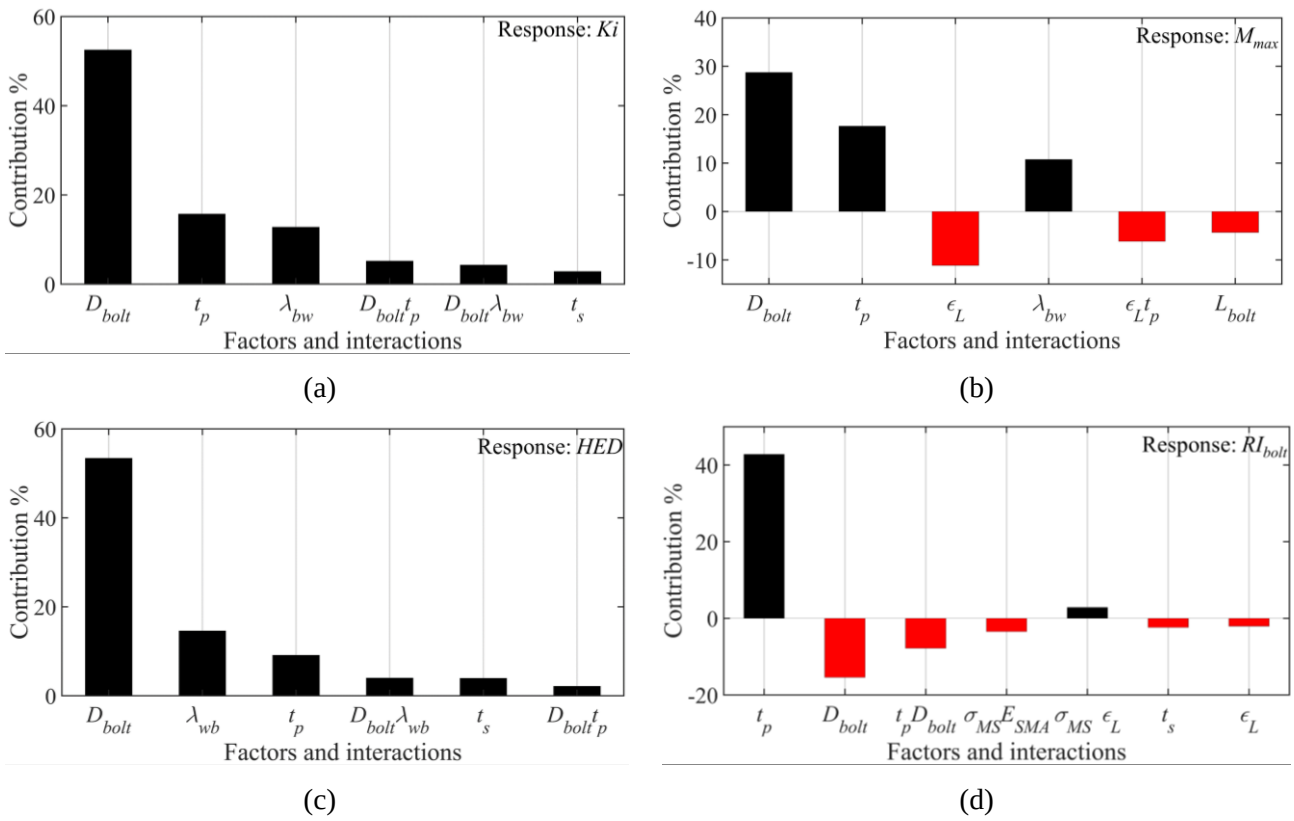

Fig. 5– The percentage contributions of significant factors and interactions on the response variables

4.1. Initial stiffness

The initial stiffness of the analyzed models broadly ranges from 5306250 kN.m/rad (model 26) to 68895520 kN.m/rad (model 28). The most influential factors on the initial stiffness are shown on Fig. 5 (a) where bolt diameter (D_{bolt}), endplate thickness (t_p), and beam web slenderness ratio (λ_{bw}) with percentage contributions of 52%, 15.7%, and 12.8%, respectively, are the most significant factors. The maximum and minimum

values of *Ki* occur in models 26 and 28, respectively. By examining the factor combinations in models 26 and 28, it is observed that D_{bolt}, t_{p}, and λ_{bw} in model 26 have their low level which lead to minimum *Ki*, whereas in model 28, these three significant factors have their maximum level result in maximum *Ki* . Stiffeners (t_{s}) also have a positive effect on the initial stiffness with a percentage contribution of 2.9%. Interactions D_{bolt} t_{p} and D_{bolt} λ_{bw} influence the *Ki* response with percentage contributions of 5.2% and 4.3%, respectively. Other factors and interactions have contributions of less than 2%.

The interaction between D_{bolt} and t_{p} is shown in Fig. 6. As it can be seen, the initial stiffness is more sensitive to the bolt diameter when the thickness of the endplate is at its high level. Based on the sensitivity analysis results, increasing the bolt diameter, endplate thickness, and beam web slenderness, i.e. beam depth, result in a higher initial stiffness.

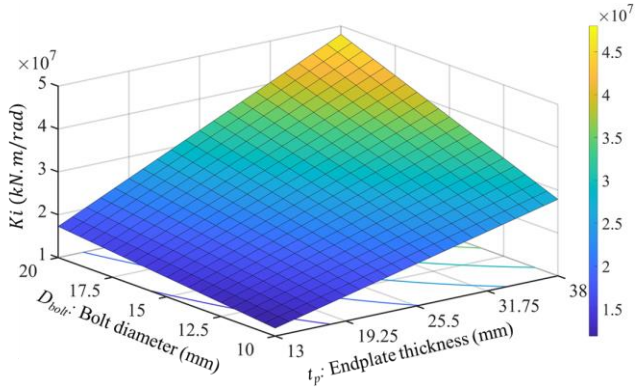

Fig. 6- The variation of the initial stiffness with respect to the bolt diameter and endplate thickness

4.2. Moment capacity

The moment capacity of the connection models analyzed varies from 64578 kN.m (in model 44) to 1107570 kN.m (in model 7). As shown in Fig. 5(b), bolt diameter (D_{bolt}), endplate thickness (t_p), and beam web slenderness ratio (λ_{bw}) have positive effects on the moment capacity of the SMA-based extended endplate connections with percentage contributions of 28.7%, 17.7%, and 10.7%, respectively. In contrast, maximum transformation strain of SMA bolts (ε_L), bolt length (L_{bolt}), and interaction $\varepsilon_L t_p$ have negative influences on the moment capacity of SMA-based connections with percentage contributions of 11.1%, 4.3%, and 6.2%, respectively.

The variation of the moment capacity with respect to the SMA maximum transformation strain and the bolt diameter is shown in Fig. 7 As shown in the 3D plot, the bolt diameter has positive effect, while the maximum transformation strain has a negative impact on the moment capacity. Based on the results, moment capacity is increased by up to 153% by increasing the bolt diameter from 10 mm to 20 mm. On the other hand, decreasing the maximum transformation strain from 13.5% to 5% increases the moment capacity by up to 73%.

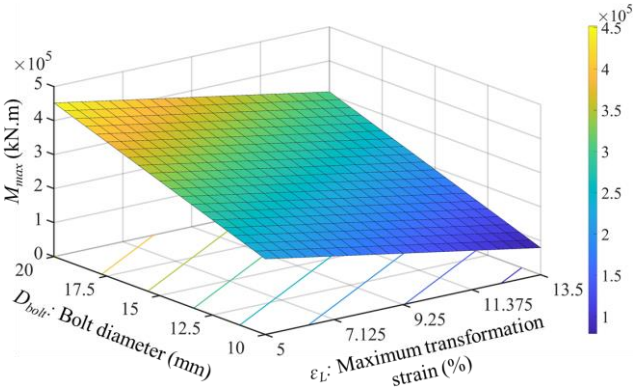

Fig. 7- The variation of the maximum applied moment with respect to the bolt diameter and maximum transformation strain

4.3 . Hysteretic energy dissipation

The absorbed energy in the analyzed models is recorded using the total area enclosed by hysteretic moment-rotation curve. Depending on the factor combinations, a wide range of *HED* is observed, i.e. from 3877.1 (kN.m.rad.) to 56326.5(kN.m.rad.) in models 26 and 7, respectively. As shown in Fig. 5(c), *HED* is mainly affected by bolt diameter (D_{bolt}), beam web slenderness ratio (λ_{bw}), and endplate thickness (t_{p}) with percentage contribution of 53.4%, 14.6%, and 9.1%, respectively. Stiffeners (t_{s}) and interaction between bolt diameter and beam web slenderness ratio (D_{bolt} λ_{bw}) have positive effects on *HED* with percentage contribution of 3.9% and 4%, respectively. Other factors and interactions have a contribution less than 3%.

The effect of interaction between the bolt diameter and the beam web slenderness ratio is shown in Fig. 8. As shown, both bolt diameter and beam web slenderness ratio have positive or increasing effect on the absorbed energy during cyclic load. It is worthy to note that the effect of bolt diameter at the high level of beam web slenderness ratio is greater. Hence, to have more energy dissipation during a seismic event using connections with larger bolt diameter and deeper beams is recommended.

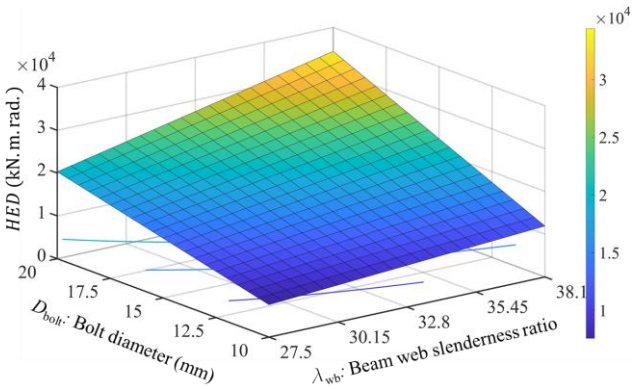

Fig. 8- The variation of the hysteretic energy dissipation with respect to the bolt diameter and beam web slenderness ratio

4.4. SMA-bolt rupture index

Rupture index is an indicator for fracture. The higher RI_{bolts}, the more potential for bolt fracture. Among sixty-four analyzed connection models, this index ranges from 0.005 to 2.46 in models 24 and 42, respectively. Previous research [3,4] shows that SMA-bolt fracture is a major issue in SMA-based steel

connections. Therefore, an especial attention should be given to early bolt fracture in SMA-based steel connections.

As shown in Fig. 5(d), RI_{bolts} is mostly influenced by endplate thickness (t_p) and bolt diameter (D_{bolt}) with percentage contributions of 42.8% and 15.4%, respectively. The RI_{bolts} response is also negatively influenced by interactions t_p D_{bolt} (percent contribution of 7.8%) and σ_{Ms} E_{SMA} (percent contribution of 3.5%). Other factors and interactions have contributions less than 3%.

The 3D surface plot in Fig. 9 shows the variation of RI_{bolts} with respect to the bolt diameter and endplate thickness. As shown, increasing the bolt diameter, and meanwhile reducing the endplate thickness lead to less RI_{bolts}. Although thinner endplate reduces the potential for the bolt fracture, a thin endplate might result in thin-plate behavior, which in turn, causes residual deformation. Therefore, reasonable ranges for bolt diameter and endplate thickness are required to avoid bolt fracture, and on the other hand, minimize the residual deformations.

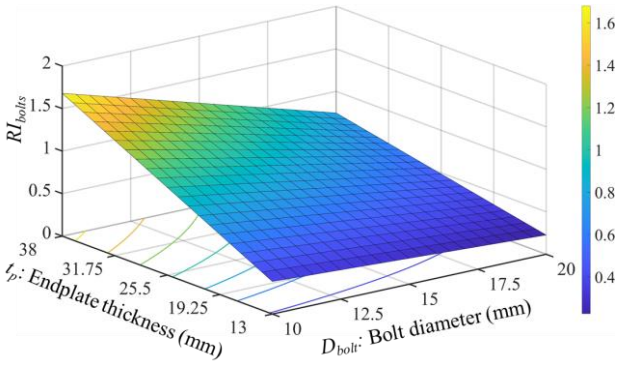

Fig. 9- The variation of the RI_{bolts} with respect to the endplate thickness and the bolt diameter

5. Summary and conclusion

This paper discussed the behavior of extended endplate connections equipped with SMA-bolts under cyclic loading. The study commenced with developing a finite element model. Then, the developed model is verified using an experimental study. The validated finite element model and design-of-experiment framework are then used to evaluate the effect of twenty-one design parameters on the cyclic response of extended endplate connections equipped with SMA-bolts. Ranges for these twenty-one design parameters were chosen to meet the seismic design requirements of AISC 358-16 and AISC 341-16 for the extended endplate moment connections. The cyclic response parameters which were considered in this study included initial stiffness (K_i), moment capacity (M_{max}), hysteretic energy dissipation (*HED*), and SMA-bolt rupture index (RI_{bolts}). The following conclusions were drawn from this study:

- Bolt diameter (D_{bolts}) and endplate thickness (t_p) are the most significant factors. D_{bolts} and t_p appear among the first three important factors for all the response variables.
- For the extended-endplate connections equipped with SMA-bolts, using thicker endplates and bolts are recommended to reach stiffer connections with the high levels of moment capacity and hysteretic energy dissipation.
- Initial stiffness is mainly influenced by bolt diameter, endplate thickness, and beam web slenderness ratio with a total percentage contribution of 80.5%.
- Energy dissipation capacity can be increased by increasing bolt diameter, beam depth, increasing the endplate thickness, and adding stiffener plates. These factors have a total variability of 81% in *HED*.

- Bolt rupture index is affected by endplate thickness, bolt diameter, and the existence of stiffener plates. The potential for bolt fracture, which is critical for SMA-based steel connections, can be reduced by increasing the bolt diameter and adding stiffeners.

Acknowledgements

The presented research is financially supported by the Natural Sciences and Engineering Research Council of Canada (NSERC) through Discovery Grant. The authors gratefully acknowledge this financial support.

Copyrights

References

[1] Ricles JM, Sause R, Garlock MM, Zhao C (2001): Posttensioned Seismic-Resistant Connections for Steel Frames. *Journal of Structural Engineering*, **127**, 113–121.

[2] Moradi S, Burton H V., Kumar I (2018): Parameterized fragility functions for controlled rocking steel braced frames. *Engineering Structures*, **176**, 254–264.

[3] Fang C, Yam MCH, Lam ACC, Xie L (2014): Cyclic performance of extended end-plate connections equipped with shape memory alloy bolts. *Journal of Constructional Steel Research*, **94**, 122–136.

[4] Wang W, Fang C, Liu J (2017): Self-Centering Beam-to-Column Connections with Combined Superelastic SMA Bolts and Steel Angles. *Journal of Structural Engineering*, **143**, 04016175.

[5] Speicher MS, DesRoches R, Leon RT (2011): Experimental results of a NiTi shape memory alloy (SMA)-based recentering beam-column connection. *Engineering Structures*, **33**, 2448–2457.

[6] Ocel J, DesRoches R, Leon RT, Hess WG, Krumme R, Hayes JR, Sweeney S (2004): Steel beam-column connections using shape memory alloys. *Journal of Structural Engineering*, **130**, 732–740.

[7] DesRoches R, Taftali B, Ellingwood BR (2010): Seismic Performance Assessment of Steel Frames with Shape Memory Alloy Connections. Part I — Analysis and Seismic Demands. *Journal of Earthquake Engineering*, **14**, 471–486.

[8] ANSYS (2018): ANSYS mechanical APDL (release 19.1). *Canonsburg (PA): ANSYS Inc*.

[9] DX11 (2018): Design-Expert® software version 11.

[10] Moradi S, Alam MS (2015): Feasibility study of utilizing superelastic shape memory alloy plates in steel beam–column connections for improved seismic performance. *Journal of Intelligent Material Systems and Structures*, **26**, 463–475.

[11] Ju H, Lin C, Liu Z, Zhang J (2018): Study of in-situ formation of Fe-Mn-Si shape memory alloy welding seam by laser welding with filler powder. *Optics and Laser Technology*, **104**, 65-72.

[12] Farmani MA, Ghassemieh M (2016): Shape memory alloy-based moment connections with superior self-centering properties. *Smart Materials and Structures*, **25**, 075028.

[13] Mohammadi Nia M, Moradi S (2020): Limit State Behavior and Response Sensitivity Analysis of Endplate Steel Connections with Shape Memory Alloy Bolts (Submitted). *Journal of Intelligent Material Systems and Structures*.

[14] Hinkelmann K (2012) *Design and Analysis of Experiments*, John Wiley & Sons, Inc., Hoboken, NJ, USA.

